In-line Near-Infrared Spectroscopy: A Tool to Monitor the Preparation of Polymer-Clay Nanocomposites in Extruders

Joana M. Barbas, Ana V. Machado, José A. Covas

Institute for Polymers and Composites and I3N, University of Minho, Campus of Azurém, 4800-058 Guimarães, Portugal
Correspondence to: J. M. Barbas (E-mail: joana.barbas@dep.uminho.pt)

Abstract

In-line diffuse reflectance and on-line transmission near-infrared spectroscopy (NIR) measurements are performed at the same location of the barrel of a twin screw extruder during the preparation of a polypropylene/clay nanocomposite. Their performance is evaluated by means of a 7-parameter chemometric model using off-line rheological and structural (FTIR) data obtained from samples prepared under different screw speed, compatibilizer content and clay loading, as well as a process-related thermomechanical index. Despite the higher variability of the diffuse reflectance signal, the two models present analogous high quality indices. The aptness of the reflectance measurements is thus validated, which has direct practical advantages, as this probe can be fixed in any typical melt pressure transducer port. The probe is then used for the real-time in-line monitoring of the production of the same nanocomposite but now using different throughputs, and the chemometric-based predictions are compared with experimental off-line characterization data. The nonlinear effect of throughput is correctly anticipated. © 2012 Wiley Periodicals, Inc. J. Appl. Polym. Sci. 127:4899-4909, 2012

KEYWORDS: in-line monitoring; near-infrared spectroscopy; polymer-clay nanocomposites; twin screw extrusion

INTRODUCTION

Polymer-clay nanocomposites exhibit excellent physical and mechanical performance at clay contents typically lower than 5% in weight. [1,2] It is currently well established that their properties are determined by the morphology and clay dispersion level and that these are strongly influenced by the conditions used for the compounding and processing stages. [1–7] However, correlations between dispersion and processing conditions remain unclear, [3–7] which continue to make difficult process set-up, optimization, control, and scale-up. Real-time monitoring of material characteristics upon compounding and processing of these materials is thus of great interest. On-line oscillatory rheometry [8] was successfully used for the characterization of polymer-clay nanocomposites along a twin screw extruder. Correlations between the rheological response and the degree of mixing could be established, but it has been reported that in some cases rheology is unable to discriminate between different dispersion levels. [6,9] Also, rheological measurements take typically a few minutes, that is, they are not performed in real time. Spectroscopic techniques, near-infrared (NIR) in particular, have found a remarkable development due to the recent advances in probes, sensor technology and equipment construction. [10–14] On-line NIR during polymer processing (usually extrusion) is mostly performed in transmission mode, using flow-cell fixtures inserted between extruder and die. [13–19] However, acquiring NIR spectra by means of reflection probes [20–23] can be more convenient, as fixing them to the processing equipment, inclusive along its axis, should be easier and allow monitoring the evolution of dispersion along the screw. Rohe et al. [20] used prototype transmittance and reflection probes during blending of polyethylene with polypropylene in a twin screw extruder and found out that they produced comparable results, even if the authors had to develop a complex optical bypass system. Curiously, most previous on-line NIR monitoring of the preparation of clay nanocomposites has been performed using reflection probes, but these have been located between extruder and die. Moghaddam et al. [21] correlated temperature, particle size, and viscosity changes of polymer-clay nanocomposites with spectral differences. Witschnigg et al. [22] studied the effect of screw speed and geometry on the final composite performance. Fischer et al. [23] correlated the spectral data with the degree of exfoliation of melt that was detoured from the main stream before crossing the die. These pioneering studies focused essentially on the clay reinforcement effects and applied a simplified chemometric analysis. The authors [24] monitored the evolution of clay dispersion during compounding in a batch mixer and attempted to develop appropriate chemometric models. For this purpose, they tested models of different complexity using

Table I. Materials Used in the Work

Material	Producer	Acronym	Grade	MFI/lamellar distance
Polypropylene	Lyondell Basell	PP	Moplen HP500N	12 g /10 min(230°C /2.16 kg)
Compatibilizer	Crompton	PP-g-MA	Polybond 3200	115 g /10 min(190°C /2.16 kg)
Montmorillonite clay	Laviosa	D67G	Dellite 67G	d_{001} = 3.70 nm

parameters derived from various well established dispersion characterization techniques. Eventually, a 7-parameter model comprising data from oscillatory rheometry, Fourier transform infrared spectroscopy (FTIR) and a thermomechanical processrelated index provided good predictive capacity.
Carrying out diffuse reflectance measurements along the axis of a twin screw extruder could involve a few complications. The periodic exposure of the probe to the rotating surfaces of the tips of the screw elements, the eventual presence of large clay solid particulates that may act as diffuse reflectors, the complex threedimensional flow pattern developing in mixing zones and the possibility that the screws will not work fully filled at the measuring point could interfere with the spectra measurement. This work aims at investigating the effectiveness of diffuse reflectance to monitor the preparation of a polypropylene/polypropylene grafted with maleic anhydride/organo-montmorillonite (PP/PP-*g*-MA/D67G) system in a twin screw extruder using commercial probes and appropriate chemometrics. In-line (not on-line) measurements at the extruder barrel are targeted, that is, without affecting material flow and performed as upstream in the process as possible. The quality of the spectra acquired by transmission and diffuse reflectance probes is first compared. Then, 7-parameter chemometric models are built for each measurement mode on the basis of characterization data from nanocomposites prepared with different screw speed, compatibilizer content, and clay content. The aptness of the two probes is compared by assessing quantitatively the quality of each model. Ultimately, the diffuse reflection probe is used for the real-time in-line monitoring of samples prepared using different throughputs, the predictions being compared with experimental off-line characterization data.

EXPERIMENTAL

Materials and Composites

The materials used in this work are listed in Table I. They include an injection molding grade polypropylene (PP), a poly-

Table II. Composition of the Various PP/PP- *g*-MA/D67G Nanocomposites Prepared

Variable	PP [wt %]	PP-g-MA [wt %]	D67G [wt %]
Reference	90	5	5
% PP-g-MA	95	0	5
	85	10	5
% clay	94	5	1
	93	5	2
	92	5	3
	87.5	5	7.5

propylene grafted with maleic anhydride (PP- g-MA) and Dellite 67G (D67G), a natural montmorillonite clay modified with dimethyl dihydrogenated tallow quaternary ammonium salt (2 M 2 HT). Table II presents the compositions of the $PP/PP-g$ MA/D67G nanocomposites prepared in a modular corotating intermeshing twin screw extruder Leistritz LSM 30.34. As NIR spectra are quite sensitive to temperature variations, [16] the barrel and die set temperature were kept constant at 200°C for all the extrusion runs. The feed rate (Q) was always set at 3 kg/h by a Moretto Dosing System DVM18-L and the reference screw speed was 100 rpm . In the case of the 90/5/5 wt % nanocomposite, various screw speeds were used (50, 100, 200, and 300 rpm).

Process Monitoring Set-Up

The NIR process monitoring system used is depicted in Figure 1 and comprises three main components:

- Two commercial sensors, a diffuse reflectance probe FDR650 and a transmission probe FPT-850 (both from Axiom Analytical). The first has a sapphire window with a diameter of 5.7 mm , for an illuminated area with a diameter of 3.2 mm and a field depth of 3 mm . It uses an 80 fiber bundle cable that splits in two 40 fiber bundles to connect to the analyzer inlet and outlet channels. The background signal is acquired prior to installation, using a spectralon diffuse reflection standard target (Bruker Optics) with a reflectivity index of 99%. The transmission probe has a physical rectangular gap of 5 mm , corresponding to the probe optical path length. The probe's inner duct is pressurized at 4 bar with N_2 to prevent humidity condensation inside the light guide channels. It uses two fiber optic cables

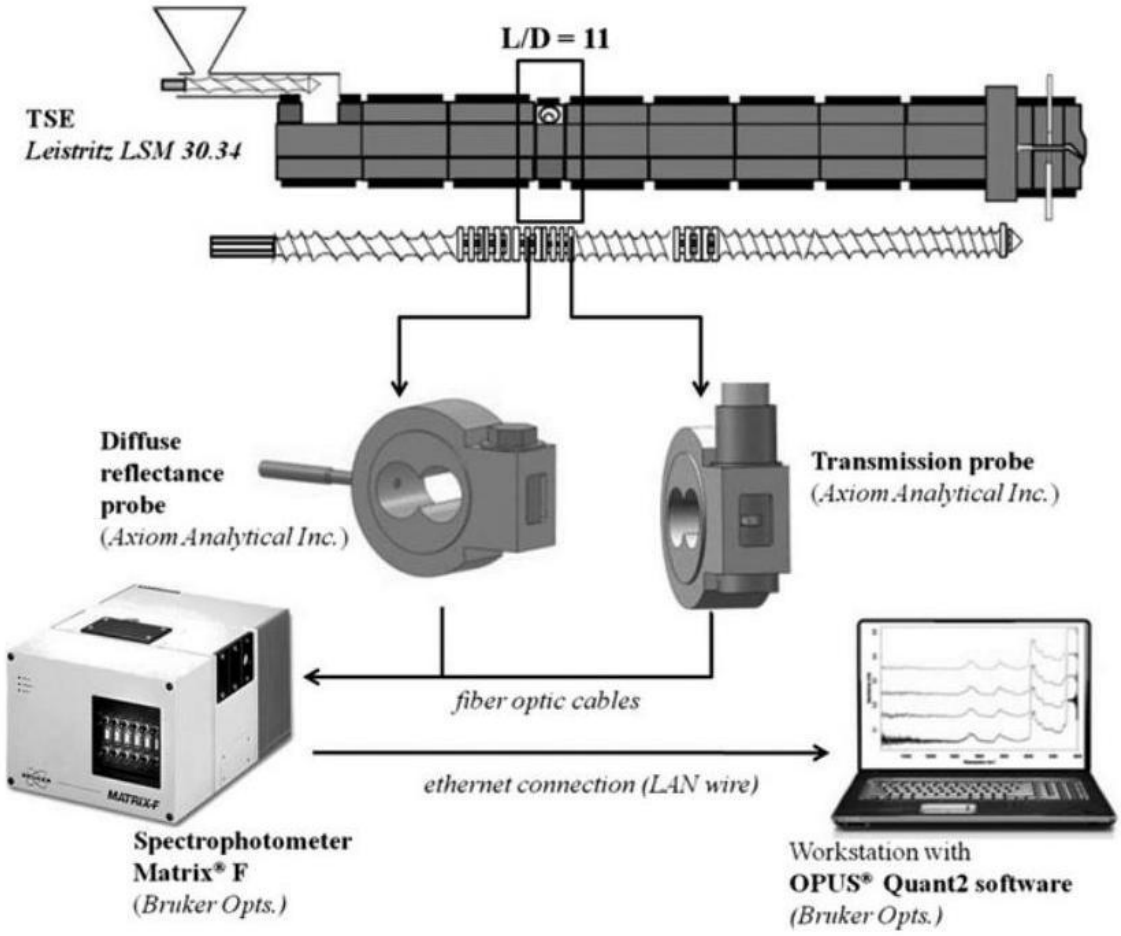

Figure 1. In-line set-up.

for the transmitting and receiving signals with a core fiber diameter of 600μ m. The background is acquired using a loop of an identical fiber optic cable.

- A Matrix [8] F (Bruker Optics) spectrometer with an InGaAs detector and a HeNe laser emitting at 633 nm at 1 mW . The scanner rate is 10 kHz .
- A PC with the OPUS ® Quant2 software (Bruker Optics) for data acquisition and analysis, communicating with the spectrometer by a LAN-type cable. The diffuse reflectance probe has a standard tip (with a 1/2 UNF thread) that enables its setting in any available conventional pressure sensor port along the extruder. The probe contacts directly the melt stream, no modifications to the extruder or die being required. The transmission probe is inserted in a modified extruder segment, [25] which consists of a bypass system developed inhouse. Whenever measurements are to be performed, a rotary valve is actuated to divert melt from within the extruder into the gap of the probe at low shear rate, to avoid any changes in morphology upon collection and measurement. In a few situations, the combined effect of the residence time in the gap and heat transfer from the cold probe surfaces (despite the sensor being embedded into a heated barrel segment) may cause cooling of the material and problems in spectra acquisition.

In the experiments reported here, the two probes were positioned at a barrel location ($L/D = 11$) corresponding to the downstream region of the first mixing zone of the screw.

The barrel segment also allows the quick collection (in circa 1 second) of material samples from within the extruder, which were then quenched and stored for subsequent off-line characterization. Thus, it could be readily confirmed that at this relatively upstream location in the process the polymer is already fully molten. Therefore, one would not only anticipate that here the evolution of dispersion is far from complete, but also that the effects of material changes and processing conditions are probably more significant. [3–5] In addition, the presence of a molten matrix is important for the subsequent rheological measurements (in fact, any remaining solids present in the sample would probably melt upon compression molding disks for the rheological measurements, i.e., the morphology of the sample upon collection would be destroyed).

Characterization of the Composites

NIR Spectroscopy (Matrix F, Bruker Optics). The NIR spectra were measured from $12{,}000 - 4500\ \mathrm{cm}^{-1}$ with a resolution of $8\ \mathrm{cm}^{-1}$ and accumulation of four scans, the acquisition time for each spectrum being less than 2 s . For comparison purposes, the spectra acquisition conditions were the same in both modes. For each sample, a total of 50 spectra were measured during 30 min of a continuous extrusion run. The NIR spectra discussed throughout this work are an average of these, without performing any further processing or signal correction.

Rotational Rheometry (AR-G2, TA Instruments). The linear viscoelastic response of the samples at 200°C was obtained from oscillatory frequency sweeps from 0.1 to 100rad/s, using parallel plates with a diameter of 25 mm and setting a 1 mm gap, performed under a constant strain (1% for the polymer and 0.5% for the composites). The disks had been previously compression molded at 200°C and 20 Tons. Considering the association between the increase of melt yield stress (σ_0) and clay exfoliation proposed by Lertwimolnum and Vergnes [3–5] and between a power law exponent (b) at low frequencies and the state of clay dispersion suggested by others, [6,9] the complex viscosity vs. frequency curves were fitted to a modified Carreau-Yasuda model with yield stress: [3–5]

$$|\eta * (\omega)| = \frac{\sigma_0}{\omega} + \eta_0[1 + \lambda\omega^a]^{\frac{(b-1)}{a}} \quad (1)$$

and to a power law [6,9] :

$$|\eta * (\omega)| = A\omega^b \quad (2)$$

where the adjustable parameters are the zero shear viscosity (η_0), the relaxation time (λ), the Yasuda parameter (a), the power law exponent (b), and the power law consistency (A). The Origin [(8)] Pro8 software was used for this purpose. The values of G′ (storage modulus) and G′′ (loss modulus) at low frequency were also determined, [3,26] as they are considered to provide a good perception of clay dispersion, with the increase of their values relating to a finer dispersion [3,26] and the formation of a plateau at low frequencies being attributed to the deformation and recovery of the dispersed particles. [26,27]

Medium FTIR (FTIR4100, Jasco). The organoclay was analyzed with a KBr mortar. The nanocomposite samples were compression molded at 200°C into $\pm 75\mu$ m thick films and analyzed in transmission mode, in the $4000 - 500\ \mathrm{cm}^{-1}$ wavenumber range with a

resolution of 4 cm^{-1}, using 32 scans. The wavenumber accuracy of the FTIR was checked prior to the measurements using the absorption peak of CO_2 at 668 cm^{-1} (background measurement, with resolution of 2 cm^{-1}, accumulation of 16 scans and apodization set to Boxcar, according to instructions of the manufacturer) for which the acceptance criterion is ± 2 cm^{-1}. Also the wavenumber repeatability was validated using a standard polystyrene film (Jasco) with thickness of 40μ m (resolution of 2 cm^{-1}, accumulation of 16 scans, and apodization set to Cosine), for which the acceptance criterion is that every reference peak is within ± 1 cm^{-1}.
The region between 1300 and 750 cm^{-1} was fitted with the Pearson VII expression using the Origin [8] Pro8 software, adjusting a 75% Gaussian shape (mu = 4) for the determination of the wavenumber shift for the 1050 cm^{-1} (Si-O in-plane) and 1080 cm^{-1} (Si-O out-of-plane) peaks. [28] The clay Si-O bond region can be decomposed at least in four peaks, three being related to the in-plane vibrations (1120,1050 , and 1020 cm^{-1}) and the fourth to the out-of-plane vibrations (1080 cm^{-1}).[28,29] As the individual clay layers become more spaced, the peaks at 1050 cm^{-1} and 1080 cm^{-1} tend to shift. When the structure is ordered and intercalated, the peak at 1050 cm^{-1} will suffer a negative shift toward a lower wavenumber, while for highly disordered or partially exfoliated morphologies the peak at 1080 cm^{-1} will shift to higher wavenumbers. [28,29]

CHEMOMETRICS

The molecular absorbance of NIR radiation is weaker than that of medium IR, enabling an analysis without sample preparation. [18,30–32] Conversely, as the response of the molecules to the exposure to NIR radiation results in complex spectra, one must rely on adequate chemometrics to extract from the data as much relevant information as possible. The correlation between the NIR spectra and the state of clay dispersion is obtained by means of a calibration model. Using the methodology developed previously and taking in its main conclusions, [24] the calibration model will include parameters derived from oscillatory rheometry (G', G'', σ_0, b), FTIR (wavenumber shift of the peaks at 1050 and 1080 cm^{-1}) and a process-related thermomechanical index, specifically the specific mechanical energy (SME), calculated as the ratio between the mechanical power consumed by the extruder (Amp) and the corresponding throughput. [33] In this study, two 7-parameter models will be calculated using either the transmission or the reflection spectra, both being built from the characterization of nanocomposites prepared with different screw speed, compatibilizer content, and clay content.

A partial least squares (PLS) regression will be applied to the calibration data set and the quality of the model is assessed by the following: [18,20,22,30–32]

- The root mean square error is calculated for all samples as:

$$\mathrm{RMSE} = \sqrt{\frac{\sum_{i=1}^{n} \left(Y_{i_{measured}} - Y_{i_{predicted}}\right)^2}{n}} \quad (3)$$

where, $Y_{measured}$ and $Y_{predicted}$ are the measured and predicted values, respectively. RMSE is usually labeled as root mean square error of estimation (RMSEE) and root mean square error of prediction (RMSEP) when applied to model development and validation, respectively. Both should be as low as possible.

- The coefficient of determination (R^2) yields the percentage of variance present in the component values that is reproduced in the subsequent prediction and is given by:

$$R^2 = \left[1 - \frac{\sum_{i=1}^{n} \left(Y_{i_{\text{predicted}}} - \overline{Y_{\text{predicted}}}\right)^2}{\sum_{i=1}^{n} \left(Y_{i_{\text{measured}}} - \overline{Y_{\text{measured}}}\right)^2}\right] \times 100 \quad (4)$$

where $\overline{Y_{\text{predicted}}}$ and $\overline{Y_{\text{measured}}}$ are the predicted and measured average values, respectively. Ideally, R^2 should be higher than 95%, but values above 90% are well accepted for qualitative studies. Low R^2 ($\ll 90\%$) may result from inappropriate reference parameters, insufficient precision of the reference data, and/or presence of outliers in the calibration data set.

- Bias is the systematic average deviation between the measured and predicted data sets:

$$\text{bias} = \frac{\sum_{i=1}^{n} \left(Y_{i_{\text{measured}}} - Y_{i_{\text{predicted}}}\right)}{n} \quad (5)$$

and should be as small as possible.

- The residual prediction deviation (RPD) is the ratio between the standard deviation of the reference values and the bias-corrected mean error of the prediction (validation step), calculated from:

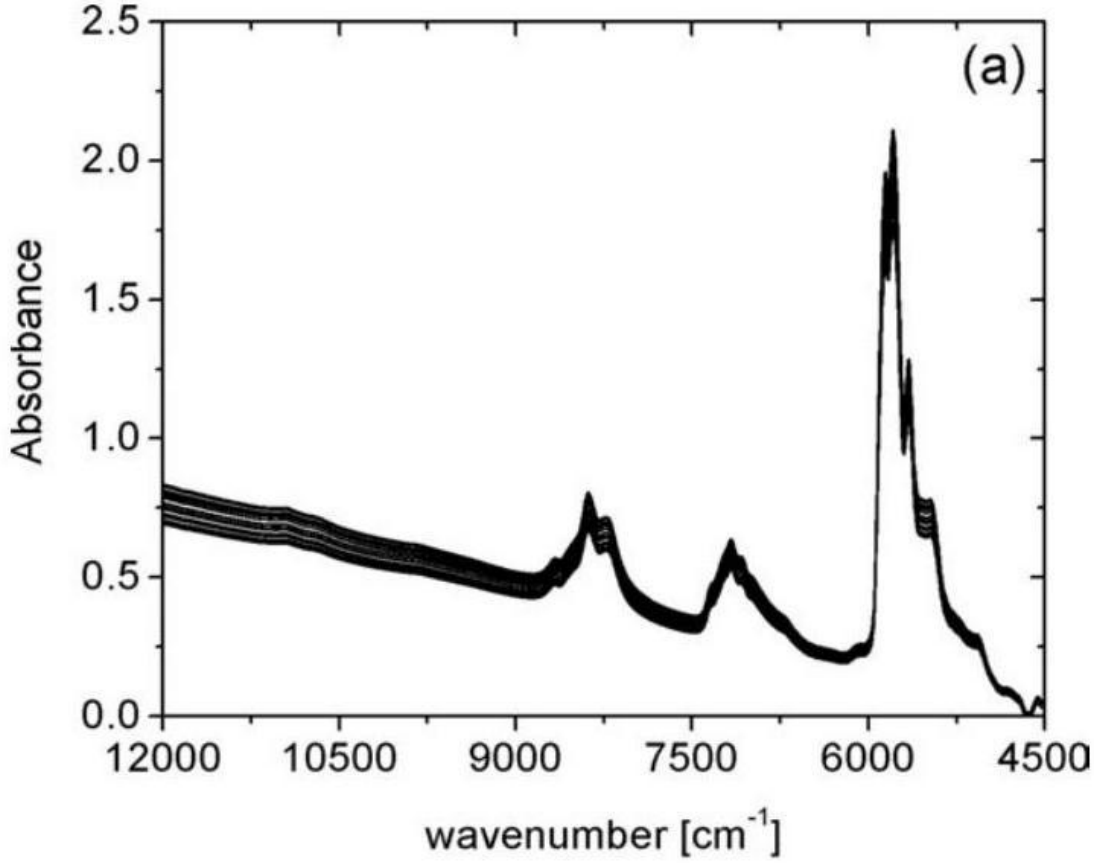
(a)
Absorbance
2.5
2.0
1.5
1.0
0.5
0.0
12000
10500
9000
7500
6000
4500
wavenumber [cm-1]

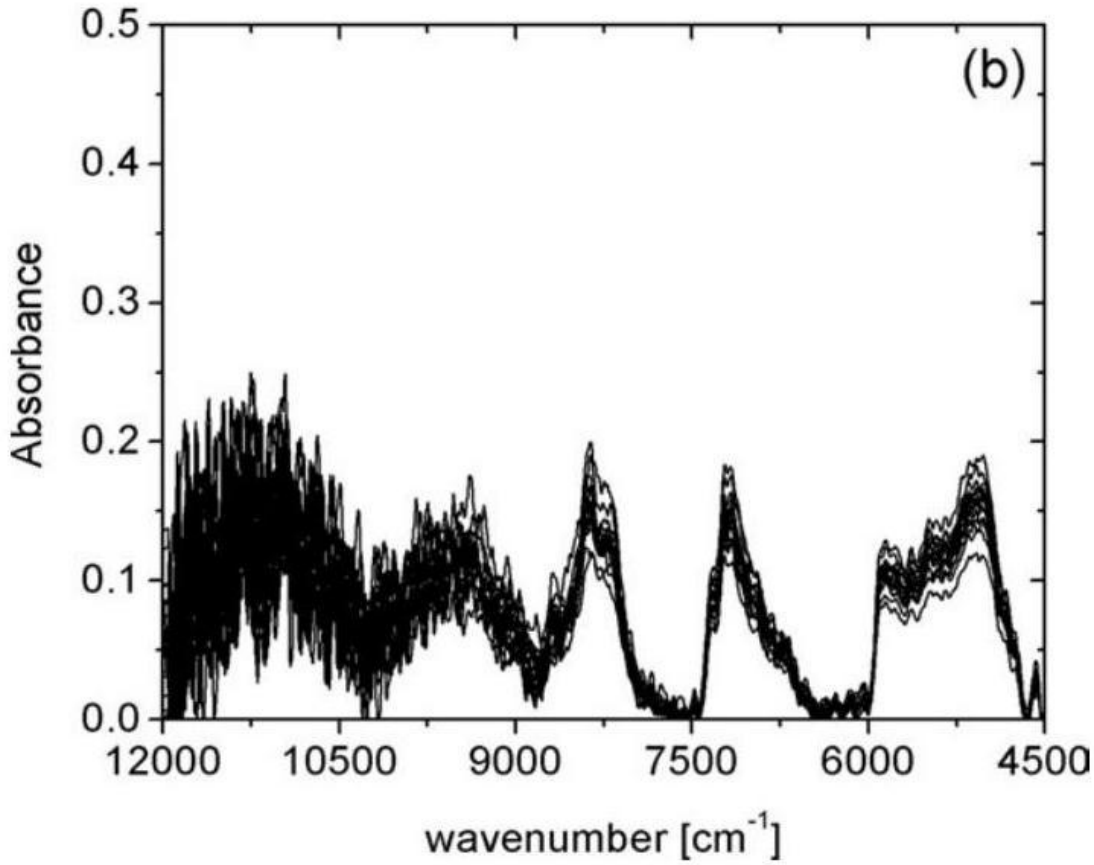
(b)
Absorbance
0.5
0.4
0.3
0.2
0.1
0.0
12000
10500
9000
7500
6000
4500
wavenumber [cm-1]

Figure 2. Spectra acquired for the 90/5/5 nanocomposite prepared at 3 kg/h and 100 rpm : (a) Transmission (b) Diffuse reflectance.

$$RPD = \frac{\sqrt{\frac{1}{M-1} \times \sum_{i=1}^{n} \left(Y_{i_{\text{measured}}} - \overline{Y_{\text{measured}}}\right)}}{\sqrt{\frac{1}{M-1} \times \sum_{i=1}^{n} \left(Y_{i_{\text{measured}}} - Y_{i_{\text{predicted}}} - bias\right)^2}} \quad (6)$$

where, M is the size of the calibration set. Values above 5 are considered as acceptable for quality control, while those over 8 indicate that the method can be used for analytical tasks.

RESULTS AND DISCUSSION

Analysis of the NIR Spectra

The signal of each spectrum (Figure 2) depends both on the chemical (molecular absorbance) and physical (scattering/reflective) characteristics of the sample, as well as on the optical measurement geometry. [30] The organic phase of the clay and the PP matrix have common spectral features, [34,35] particularly in the region between $6000 - 5000\ \text{cm}^{-1}$ assigned to the first overtone of the stretching vibrations of the CH_2 and CH_3 groups. In the PP matrix spectrum, the band at $7160\ \text{cm}^{-1}$ is assigned to the combination of first overtones and fundamental vibrations also of the CH_2 and CH_3 groups, while the band between 8400-8200 cm^{-1} corresponds to the second and third overtones of the same CH bonds. [35] The peak around $5250\ \text{cm}^{-1}$ in the

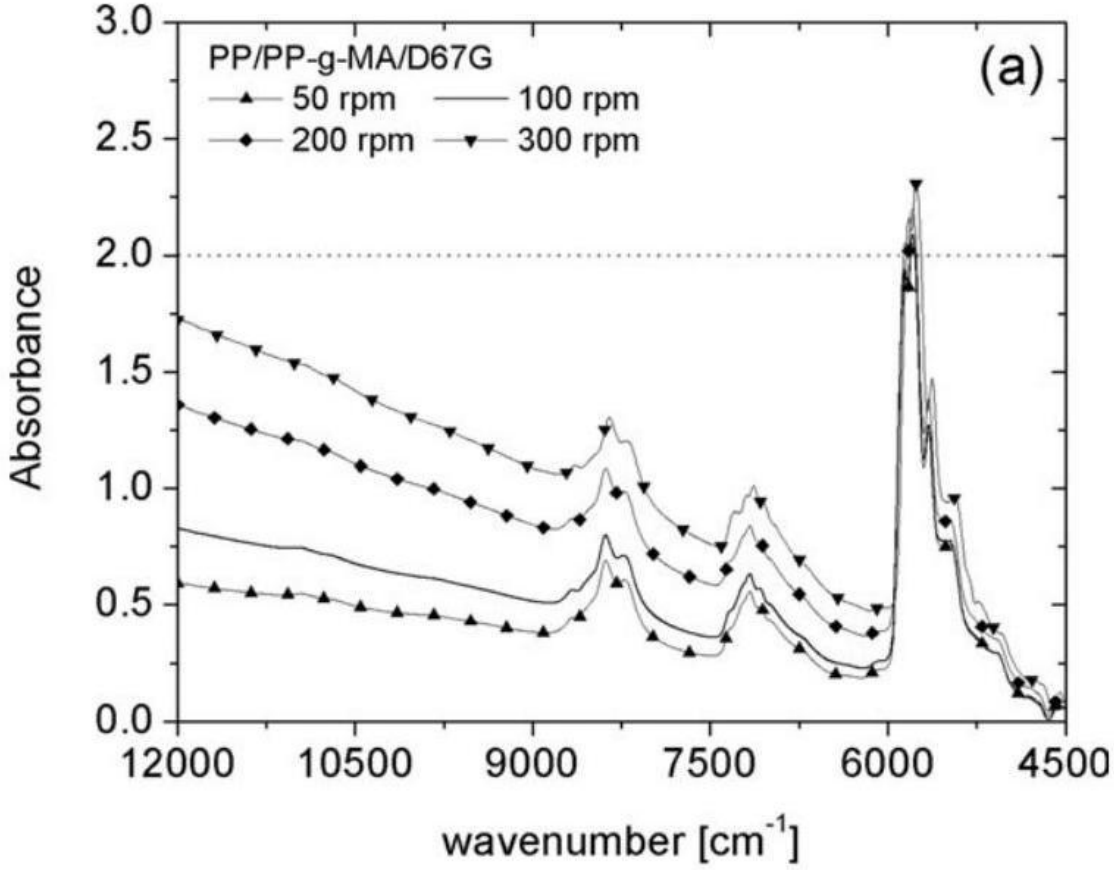
PP/PP-g-MA/D67G
50 rpm
100 rpm
200 rpm
300 rpm
(a)
Absorbance
3.0
2.5
2.0
1.5
1.0
0.5
0.0
12000
10500
9000
7500
6000
4500
wavenumber [cm-1]

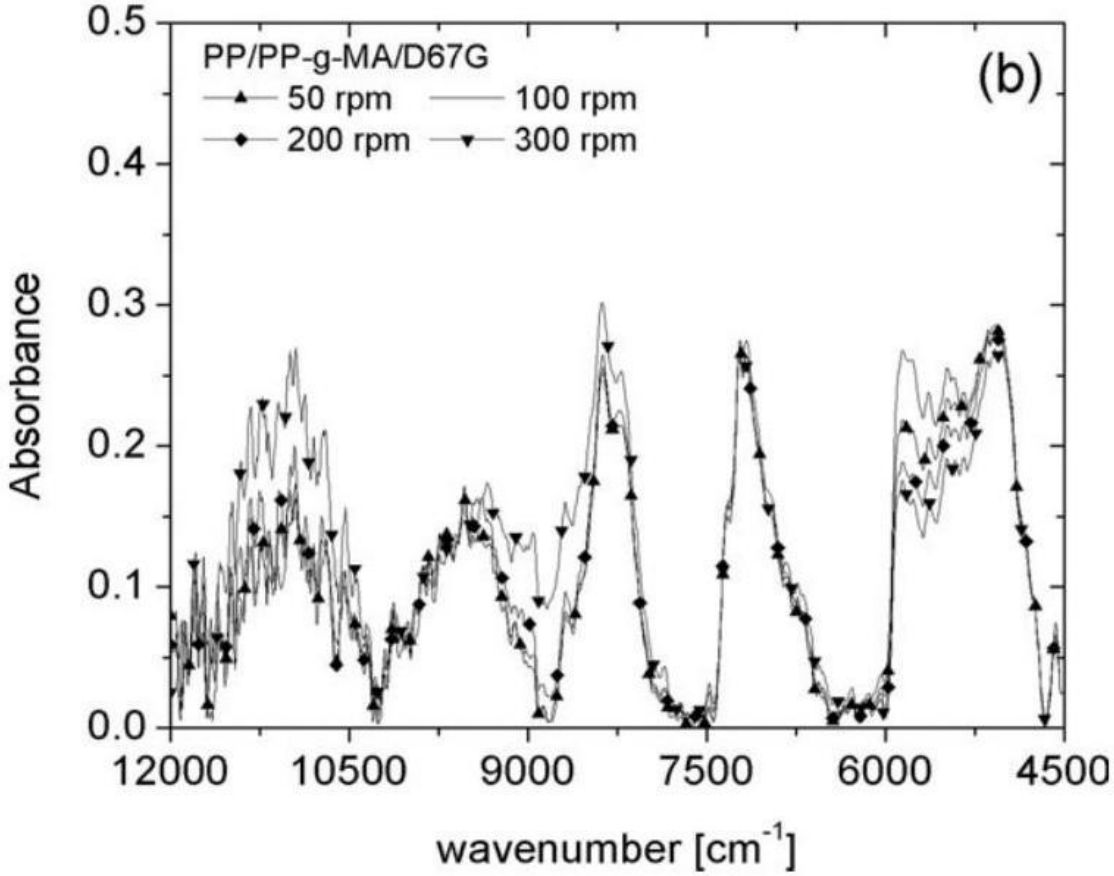
PP/PP-g-MA/D67G
50 rpm
100 rpm
200 rpm
300 rpm
(b)
Absorbance
0.5
0.4
0.3
0.2
0.1
0.0
12000
10500
9000
7500
6000
4500
wavenumber [cm-1]

Figure 3. Spectra acquired for the composites prepared with different screw speeds: (a) Transmission (b) Diffuse reflectance.
organoclay spectrum is due to the combination of stretching and bending of the water molecules. At wavelengths higher than 6500 cm^{-1} the organoclay shows a prominent band between $7200 - 6800$ cm^{-1} related to OH stretching and bending of both H_2O molecules and hydroxyls of the cationic surfactant. [34] The peak at 8230 cm^{-1} is assigned to the CH stretching vibrations of the organic phase. Due the overlapping of typical peaks and also to the low concentration of organoclay used, direct analysis of the NIR spectra of the resulting nanocomposites is sometimes difficult.

Figure 2 displays the 50 spectra as measured in transmittance and in diffuse reflectance modes for the 90/5/5 nanocomposite prepared at 3 kg/h and 100 rpm (the results are identical for the remaining samples). The stability and repeatability of the NIR signal are good, even in the region with lower signal-tonoise ratio (above 10,000 cm^{-1}). The amplitude between the maximum and minimum absorbance values is about 12% and 20% in transmission and reflection, respectively. Measurements with the diffuse reflectance probe were performed on an empty extruder operating at the same condition and the maximum absorbance values were less than 0.1% of those measured for the melt. Thus, the influence of the rotation of the screw mixing elements is negligible. Consequently, the higher variability of the diffuse reflectance signal can be attributed to scattering effects caused by clay size, number, and distribution. [30,32] The lower information depth of the diffuse reflectance signal as compared with the transmission path length may enhance this effect.

Figures 3-5 show the average spectra in transmission and reflecttance modes, without any normalization, for all the nanocomposited prepared. Figure 3 refers to PP/PP-g-MA/D67G 90/5/5 wt % prepared under different screw speeds, Figure 4 to compositions with varying compatibilizer content (from 0 to 10 wt %) and Figure 5 to nanocomposites with diverse clay content (from 1 to 7.5wt%). The region between 9000 and 5000 cm^{-1} is similar in the two modes, nonetheless signal variations in transmission are more pronounced. In the lower wavenumber region ($6000 - 4500$ cm^{-1}) the reflection spectra have worse definition, while the transmission signal shows some saturation (absorbance above 2.0). This is particularly noticeable in Figure 3(a) for the nanocomposites prepared at 200 and 300 rpm , in Figure 4(a) for the nanocomposite prepared with 10wt% PP- g MA and in Figure 5(a) for the nanocomposite prepared with 1% in weight of D67G.

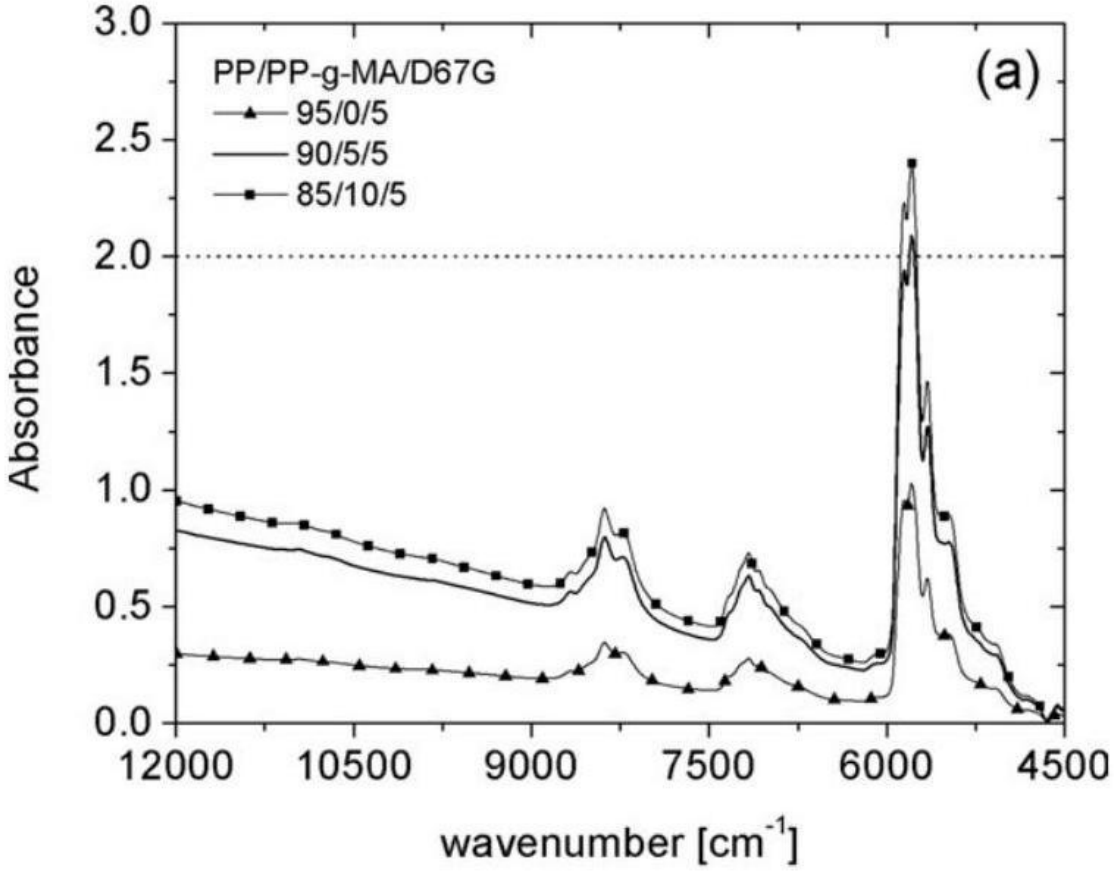
PP/PP-g-MA/D67G
95/0/5
90/5/5
85/10/5
(a)
Absorbance
3.0
2.5
2.0
1.5
1.0
0.5
0.0
12000
10500
9000
7500
6000
4500
wavenumber [cm-1]

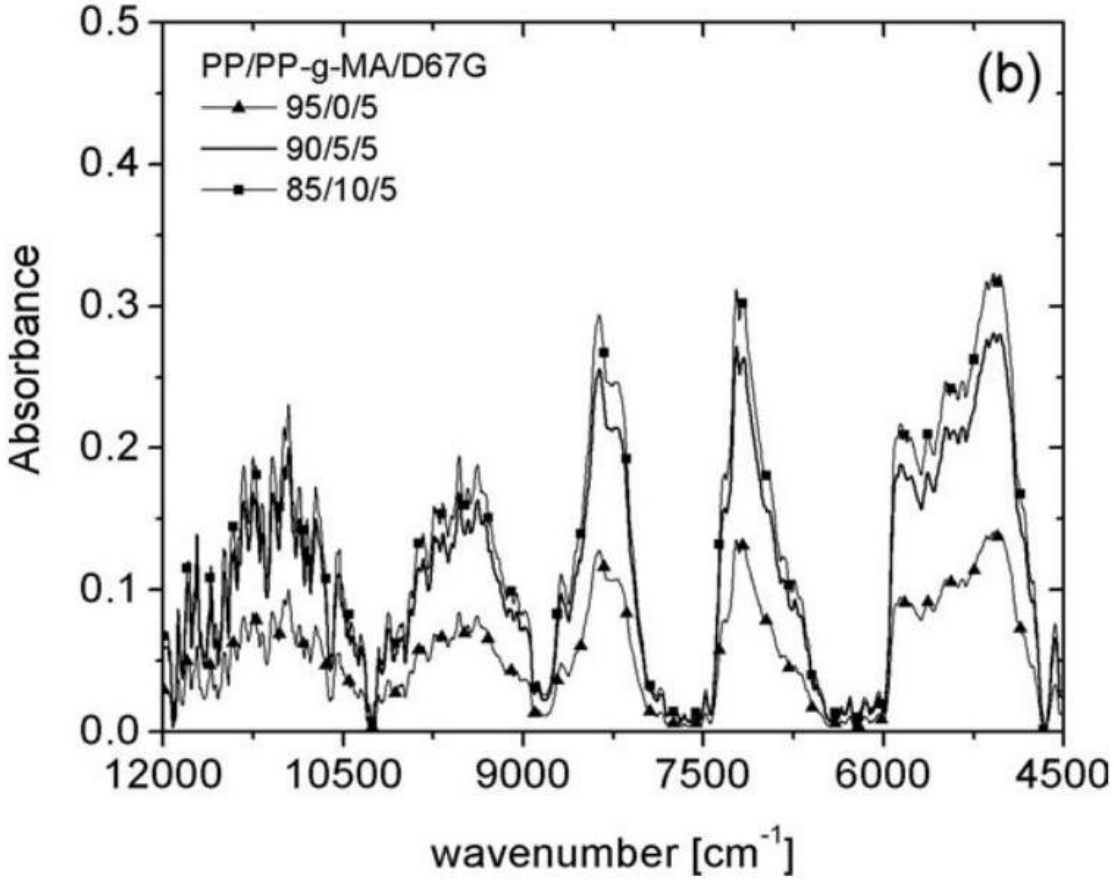
PP/PP-g-MA/D67G
95/0/5
90/5/5
85/10/5
(b)
Absorbance
0.5
0.4
0.3
0.2
0.1
0.0
12000
10500
9000
7500
6000
4500
wavenumber [cm-1]

Figure 4. Spectra acquired for the composites prepared with different PP-*g*-MA content: (a) Transmission (b) Diffuse reflectance.

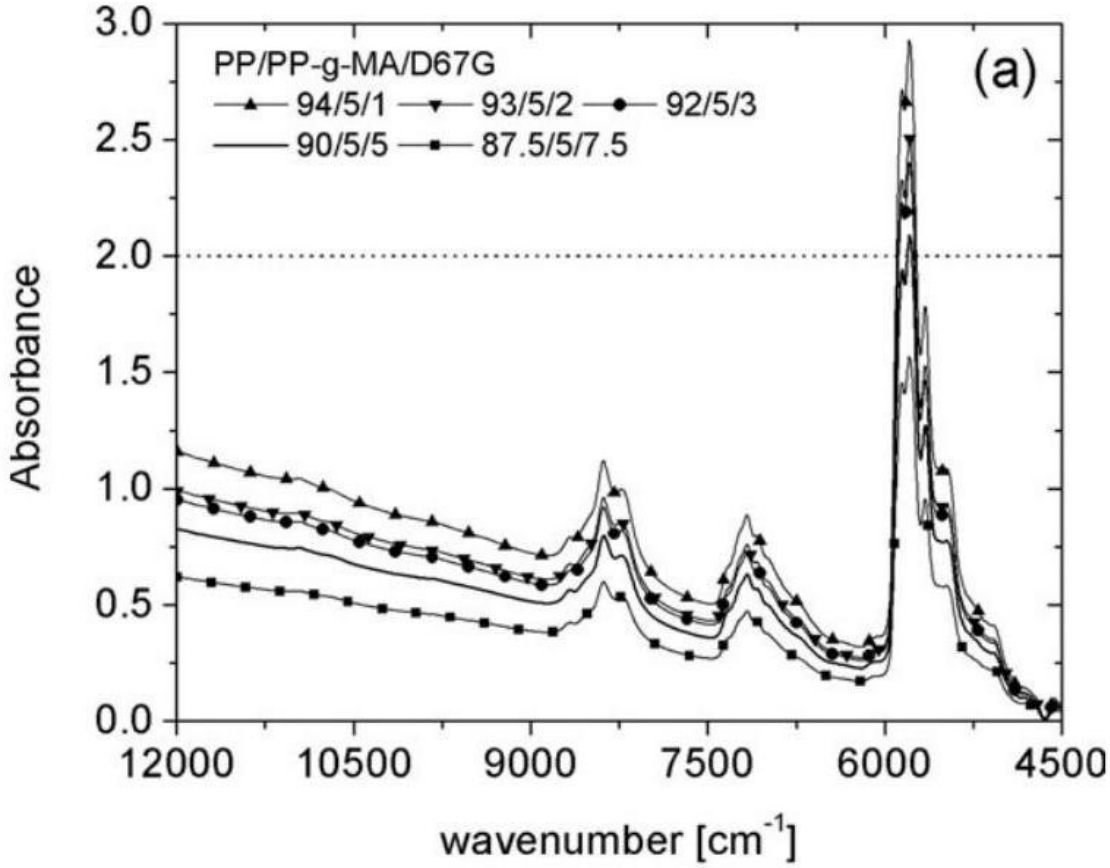
PP/PP-g-MA/D67G
94/5/1
93/5/2
92/5/3
90/5/5
87.5/5/7.5
(a)
Absorbance
wavenumber [cm-1]
3.0
2.5
2.0
1.5
1.0
0.5
0.0
12000
10500
9000
7500
6000
4500

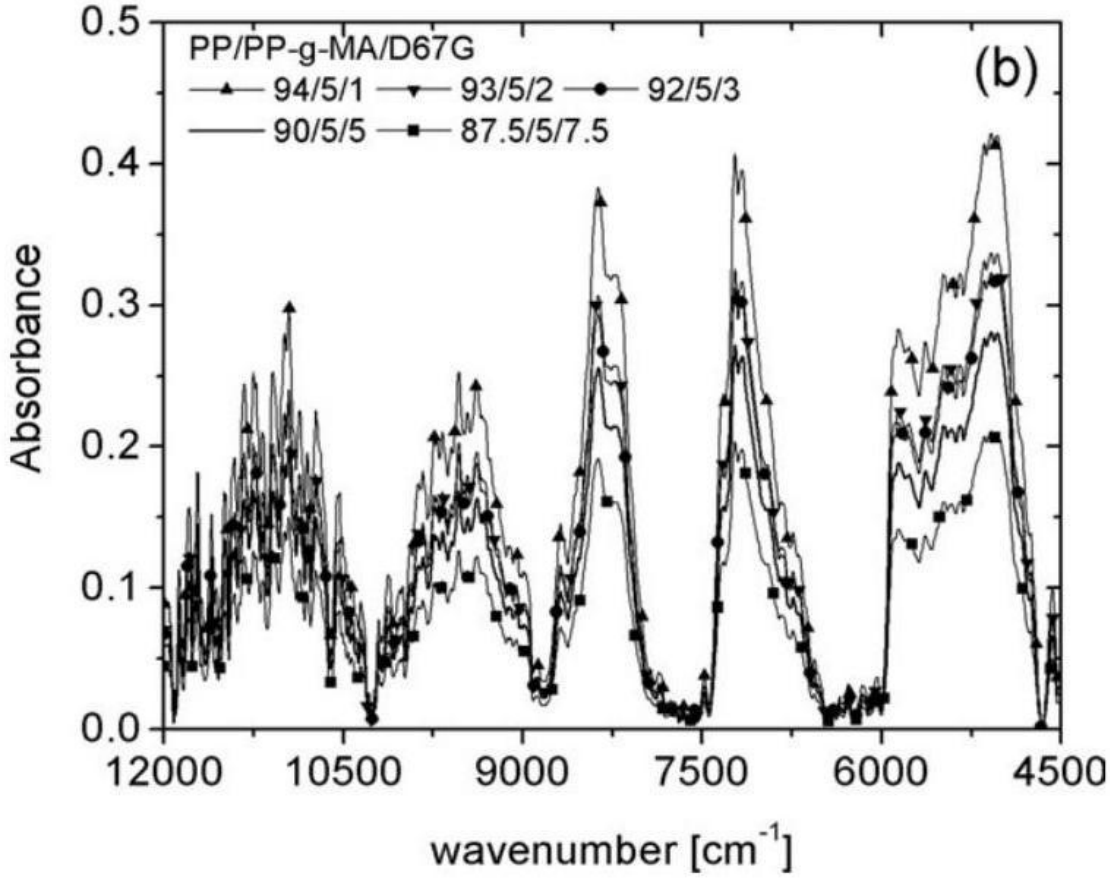
PP/PP-g-MA/D67G
94/5/1
93/5/2
92/5/3
90/5/5
87.5/5/7.5
(b)
Absorbance
wavenumber [cm-1]
0.5
0.4
0.3
0.2
0.1
0.0
12000
10500
9000
7500
6000
4500

Figure 5. Spectra acquired for the composites prepared with different clay content: (a) Transmission (b) Diffuse reflectance.

Usually, scattering increases with decreasing particle size resulting in signal losses in transmission mode and in the decrease of the signal-to-noise ratio in diffuse reflectance. Therefore, reflective losses may originate significant signal changes that are not directly related to chemical information but rather to particle distribution. [30] The spectral differences may result from a combination of clay intercalation/exfoliation, which generate a larger number of particles (clay stacks) with smaller sizes and higher interlamellar distance. In transmission mode, the baseline has a tendency to rise with increasing screw speed, increasing PP- g MA content and decreasing clay content. Anyway, the two signals become more intense with increasing screw speed, increasing PP-g-MA content and decreasing clay content, which not only demonstrates the sensitivity of the spectra to changes in the extent of dispersion, but also supports the general idea that the higher the degree of dispersion the more intense the signal becomes. As the aim is to compare the signals obtained with the two probes, to establish whether diffuse reflectance can provide the same bulk information as transmission, the analysis of the NIR spectra at this point is only qualitative.

Determining the Model Parameters

The chemometric model relates the spectral data with the clay dispersion level by means of a number of parameters that are derived from reference characterization techniques. This section presents and discusses the rheological response and medium infrared spectra obtained by the off-line characterization of the samples collected during compounding. As an example of the results obtained, Figure 6 presents the isothermal (at 200°C) linear viscoelastic response of the nanocomposites prepared under different mixing speeds. Table III brings together the values of the dynamic moduli (G' and G'') at a constant frequency of 0.1rad/s, melt yield stress (σ_0) and power law exponent (b) - see eqs. (1) and (2) - for all the experiments performed, which were designed to uncover the effect of screw speed, compatibilizer content, and clay percentage on dispersion.

The data for G' show the development of a plateau at low frequencies, a simultaneous vanishing of the Newtonian viscosity plateau at low deformation rates, as well as an increase in the overall modulus with increasing screw speed up to 200 rpm , which are usually taken as indicators of increasing dispersion levels. [1,3,26] Indeed, the solid-like behavior at low frequencies is generally attributed to the development of a percolating physical

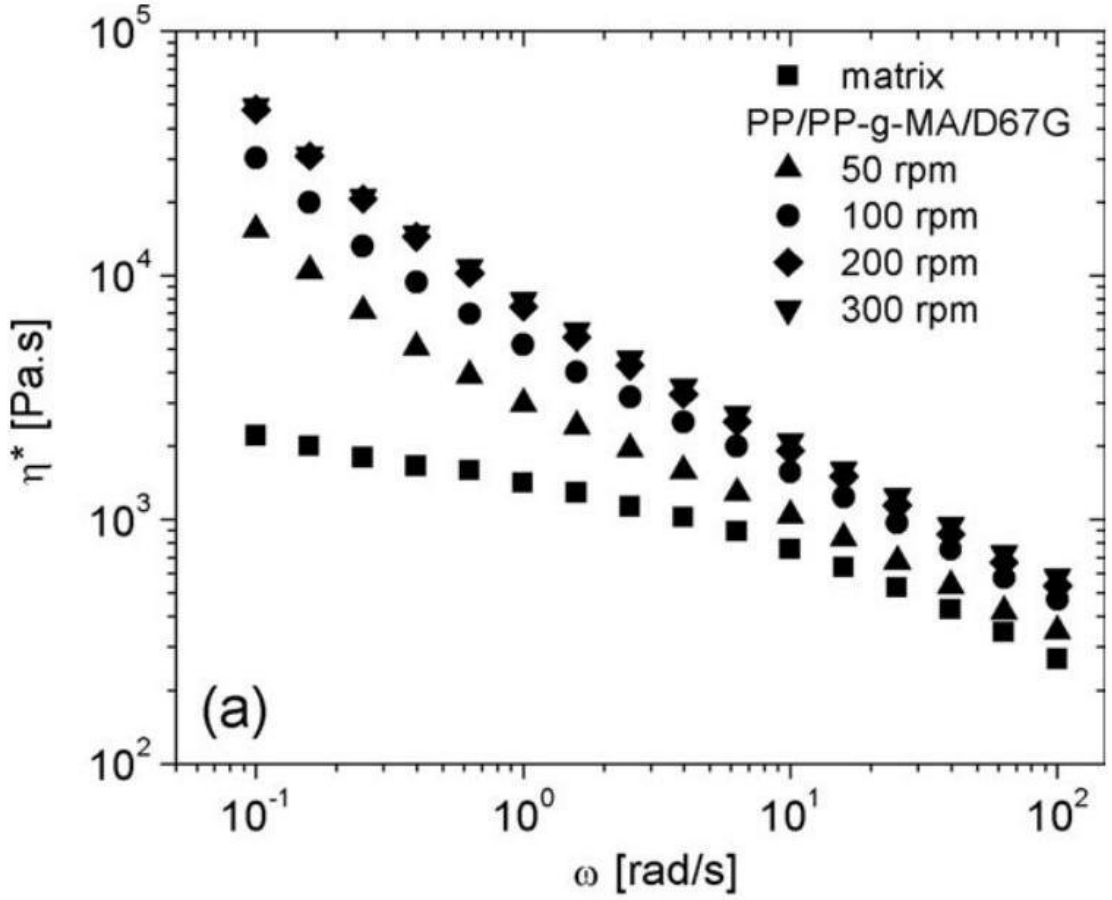
matrix
PP/PP-g-MA/D67G
50 rpm
100 rpm
200 rpm
300 rpm
(a)
η* [Pa.s]
ω [rad/s]

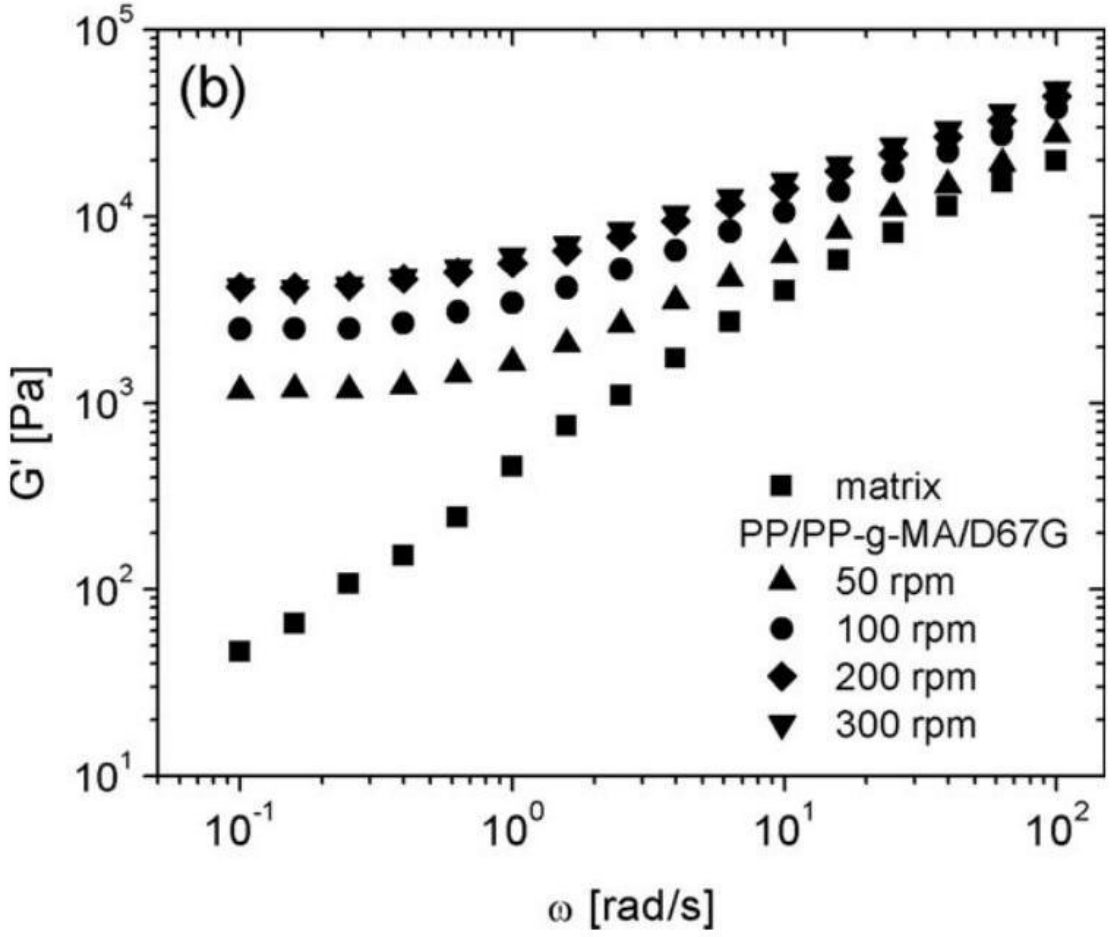
(b)
matrix
PP/PP-g-MA/D67G
50 rpm
100 rpm
200 rpm
300 rpm
G' [Pa]
ω [rad/s]

Figure 6. Linear viscoelastic response against frequency of the nanocomposites prepared with different screw speeds: (a) complex viscosity and (b) storage modulus.

Table III. Values of the Properties of the 7-Parameter Model for the Range of Compounding Runs

Sample	G′[kPa]	G′′[kPa]	σ_0[kPa]	b	1050 cm^{-1}	1080 cm^{-1}	SME
Matrix	0.046	0.215	0	-0.099	0	0	2.0
Reference	2.489	1.586	2.736	-0.832	-5.6	1	2.3
N (rpm)							
50	1.162	0.992	1.337	-0.774	-4.6	0.8	2.0
200	4.173	2.297	4.393	-0.863	-5.6	0.8	2.3
300	4.179	2.547	4.480	-0.859	-4.6	0.7	2.7
PP-g-MA (wt %)							
0	0.118	0.409	0.007	-0.102	-5.1	0	2.7
10	1.386	1.231	1.468	-0.641	-6.3	1.4	2.3
Clay (wt %)							
1	0.0731	0.294	0.072	-0.198	-13.8	1.4	2.0
2	0.432	0.694	0.793	-0.489	-14.2	2.3	2.0
3	0.572	0.716	1.027	-0.526	-14	1.5	2.3

7.5	5.726	3.022	5.786	-0.893	-5.8	0.3	2.7

clay network [27] that can be attained with increasing dispersion and/or increasing clay content. Table III demonstrates that melt yield stress (σ_0) and power law exponent (b) have a similar dependence, that is, their absolute values increase with increasing speed up to 200 rpm , no differences being perceived for 300 rpm. This probably means that the effect of the higher dynamic stresses at the highest speed is offset by the decrease of the time the material is subjected to them.

For the same samples of Figures 6 and 7 represents the FTIR spectra in the region of interest (Si-O bond) and the resultant peaks after fitting. Table III lists the wavenumber shifts at 1050 and 1080 cm^{-1}. FTIR seems to be little sensitive to changes in screw speed. The peak at 1050 cm^{-1} shifts lower wavenumbers when the speed increases from 50 to 100 rpm , which is often associated with the presence of an ordered and intercalated structure, [28,29] no other evolution being observed for higher screw speeds. The peak at 1080 cm^{-1} shows a very small positive shift that sustains the same conclusion. Nanocomposites with lower clay content (from 1 to 3wt%) show a pronounced negative shift of the peak at 1050 cm^{-1}, which can be related to higher levels of intercalation. The same samples exhibit higher shifts of the peak at 1080 cm^{-1}, indicating that partial exfoliation was attained. This suggests that the majority of samples prepared have ordered intercalated structures, but when the clay content decreases the morphologies seem to be more disordered and with higher intercalation levels, or even partially exfoliated clay platelets.

Finally, Table III also contains data on SME, the SME index. The nature of this parameter is quite different from the remaining, as it integrates the mechanical power consumed along the entire screw length - which in principle should be proportional to the mixing intensity, hence, to the dispersion level, divided by the mass output for normalization purposes. Taking again screw speed for discussion, SME increases from 2.0 to 2.7 as it goes from 50 to 300 rpm . The same type of variation was detected for the other effects studied.

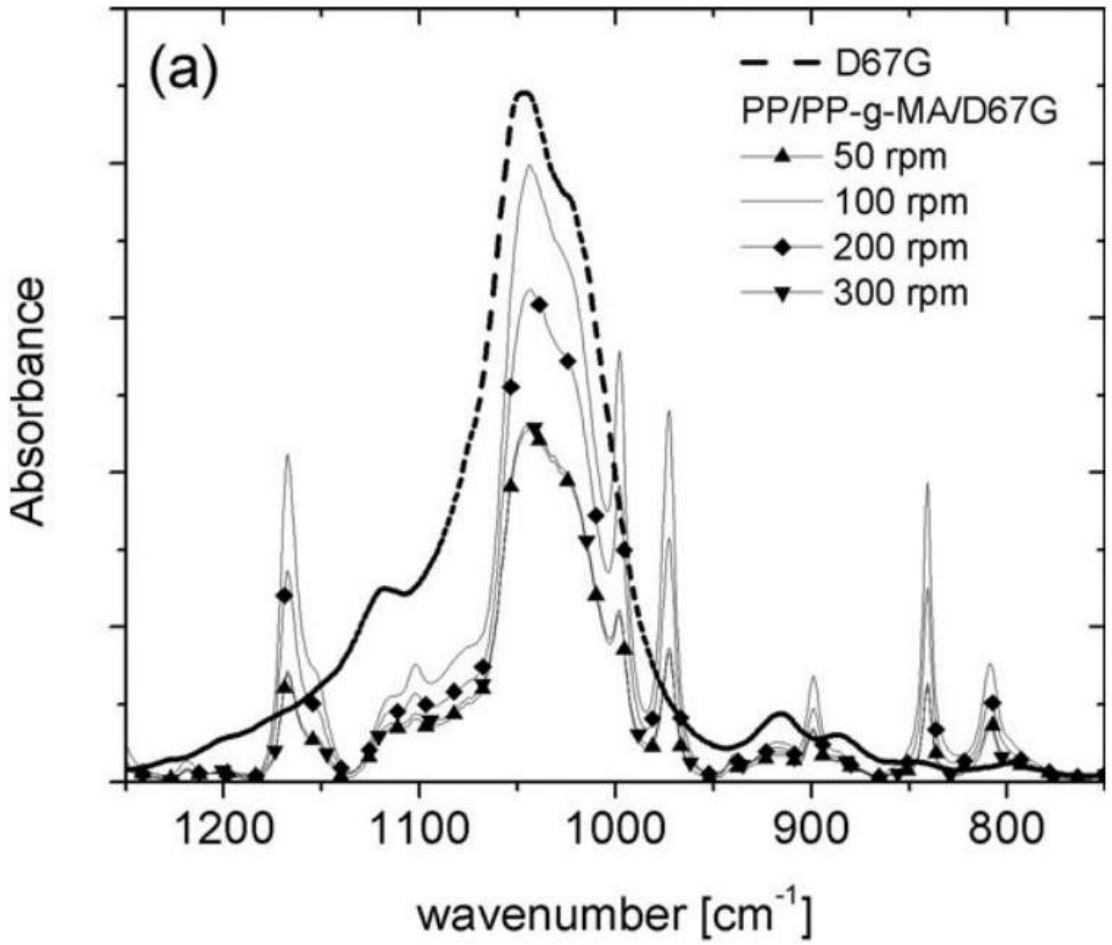
(a)
D67G
PP/PP-g-MA/D67G
50 rpm
100 rpm
200 rpm
300 rpm
Absorbance
1200
1100
1000
900
800
wavenumber [cm-1]

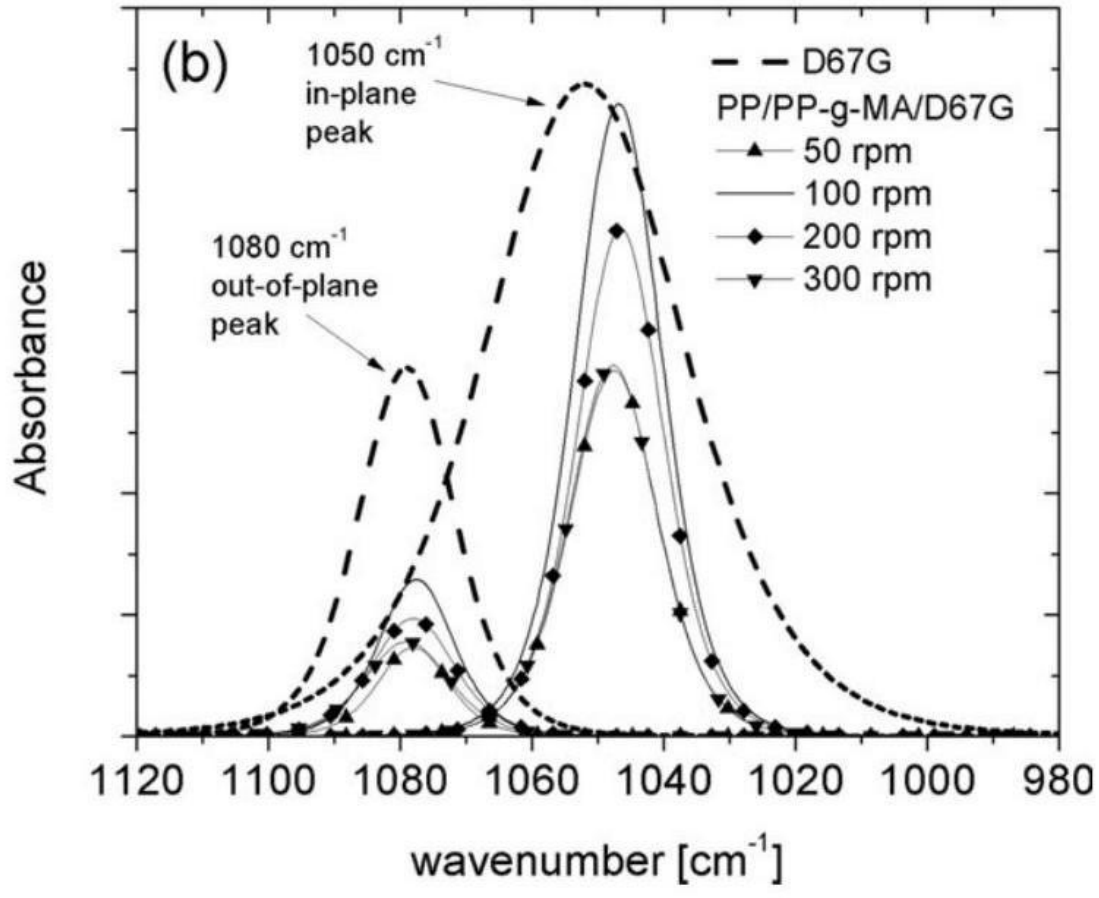
(b)
1050 cm-1
in-plane
peak
1080 cm-1
out-of-plane
peak
D67G
PP/PP-g-MA/D67G
50 rpm
100 rpm
200 rpm
300 rpm
Absorbance
1120
1100
1080
1060
1040
1020
1000
980
wavenumber [cm-1]

Figure 7. FTIR spectra in the Si – O band region of the nanocomposites prepared with different screw speeds: (a) as measured; (b) 1050 and 1080 cm^{-1} fitted peaks.

Table IV. Normalized Average Values Associated to Each of the Nanocomposites Prepared

			PP-g-MA [wt %]		Clay [wt %]			N [rpm]		
	Matrix	Reference	0	10	1	2	3	7.5	50	200	300
Normalized average [%]	0.0	51.0	20.7	43.1	25.0	41.0	43.6	79.1	31.8	62.3	70.3

Table V. Calibration and Validation Results for the 7-Parameter Models

	Calibration			Validation		
	R^2[%]	RMSEE	RPD	R^2[%]	RMSEP	bias
Transmission	98.9	1.18	11.7	98.7	1.26	-0.901
Reflection	98.9	1.21	11.6	97.8	1.45	-0.945

A detailed analysis of Table III may evidence some incoherency between the data trends indicated by the different techniques. This can be due to differences in the area analyzed, to the length scale probed by the characterized parameter, or to its particular correlation with clay dispersion. Therefore, the information provided by the various techniques selected for the 7-parameter model is complementary and offers a broad insight into the state of clay dispersion. To develop the chemometric models each parameter in Table III was normalized according to:

Normalized Average(%)

$$= \frac{(\text{Value} - \text{minimum value})}{(\text{Maximum value} - \text{minimum value})} \times 100 \quad (7)$$

That is, a score of 0% matches the polymer matrix, while 100% refers to the most dispersed nanocomposite. Table IV lists the normalized averages (representing the relative degree of dispersion) for all nanocomposites and compounding conditions used to set the calibration models. An analysis of the effect of using weights affecting the parameters linked to Rheology, FTIR, and SME revealed that a simple average of the seven parameters would yield the best results. Yet, as the number of parameters associated to each technique is different, the 7-parameter model inherently attributes more importance to rheological

data and less to SME. In a separate study, [24] it was demonstrated that this 7-parameter model has higher quality features than models purely based on rheology or FTIR data.

Transmission vs. Reflection On-Line Measurements

When applying a PLS regression to the development of a chemometric model, the optimization of its performance may include different strategies. One is to apply data preprocessing techniques, such as corrections and normalizations, to maximize the analyte specific information or the spectra distinctive features. Another is to select the spectral region that provides better selectivity. It is also important to define the optimal matrix dimension (number of factors, ranging between 1 and 10) for adequate calibration and predictive performance. [30,31] Due to the differences in signal quality pointed out in the analysis of the NIR spectra, the calibration model for transmission the mode uses four PLS factors in the spectral region between 9597.7 and 4497.4 cm^{-1} after applying vector normalization as signal correction, while for diffuse reflectance mode seven PLS factors are used and the region of interest ranges from 7502.1 to 4597.7 cm^{-1}, with a multiplicative scattering correction of the original signal. Vector normalization eliminates the effects of material density, sample thickness, and others that may influence the bands height, resulting in inaccurate information related to signal intensity. The multiplicative scattering correction is often applied to diffuse reflectance measurements to reduce the drift effects discussed before. [22,30] The Opus [(1)] Quant2 software was

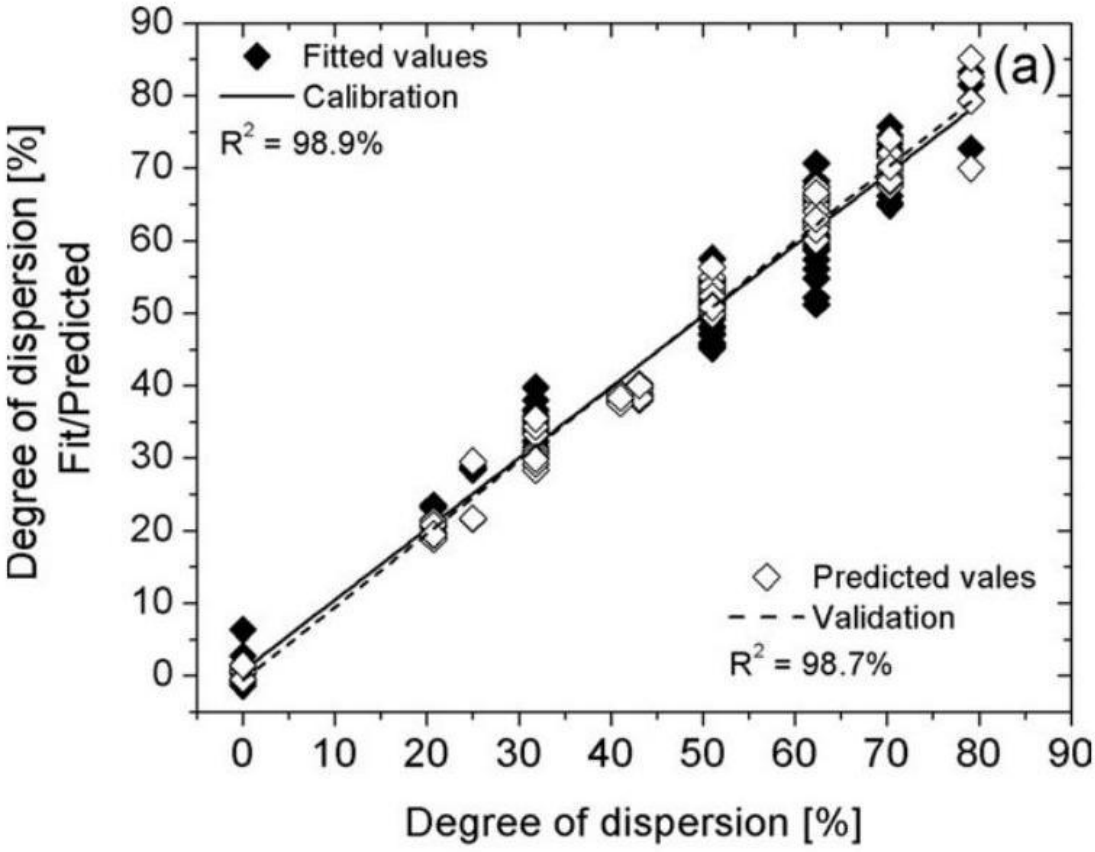
(a)
Fitted values
Calibration
R² = 98.9%
Predicted vales
Validation
R² = 98.7%
Degree of dispersion [%]
Fit/Predicted
Degree of dispersion [%]
0
10
20
30
40
50
60
70
80
90

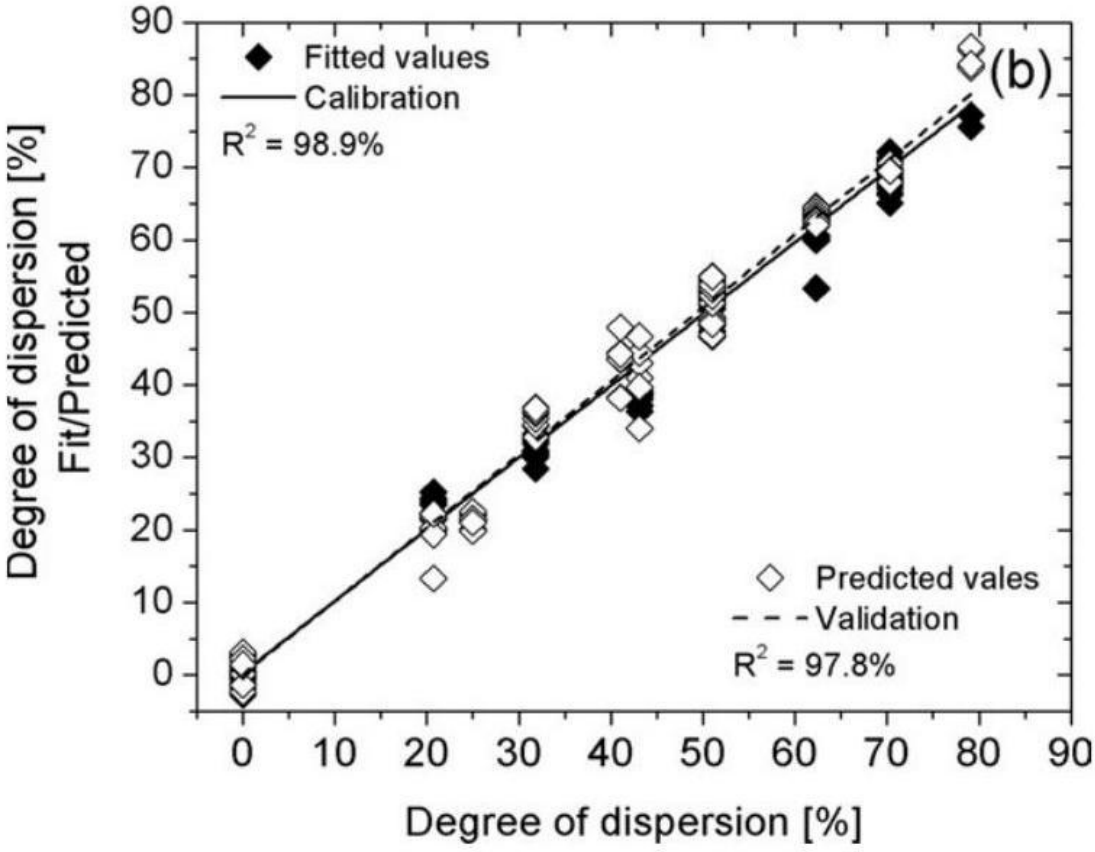
(b)
Fitted values
Calibration
R² = 98.9%
Predicted vales
Validation
R² = 97.8%
Degree of dispersion [%]
Fit/Predicted
Degree of dispersion [%]
0
10
20
30
40
50
60
70
80
90

Figure 8. Calibration models: (a) Transmission; (b) Reflection.

Table VI. Final Dispersion Levels of Nanocomposites Prepared Using Different Throughput

		Relative degree of dispersion (± error)-%		
Q [kg/h]	1.5	3	6	9
NIR prediction	32.0(±1.7)	51.6(±1.1)	73.0(±3.5)	35.4(±4.2)
Normalized average	30.1(±3.8)	51.0(±3.2)	70.1(±3.8)	40.4(±4.0)

used to run the optimization algorithms, identify the potentially best procedure, set the number of factors (pairs of scores and loadings) of the spectral matrix, select the spectral region, perform signal correction, and pinpoint eventual outliers in the test series.

Table V shows the quality factors of the models for the two measurement modes. The corresponding calibration and validatimon curves are illustrated in Figure 8. The validation/calibration population ratio was kept at 15%.[24] The two measurement modes yielded good quality models, with R^2 values higher than 95% for calibration and validation. The RMSEP values are low and very similar, while the RPD values are identical and above

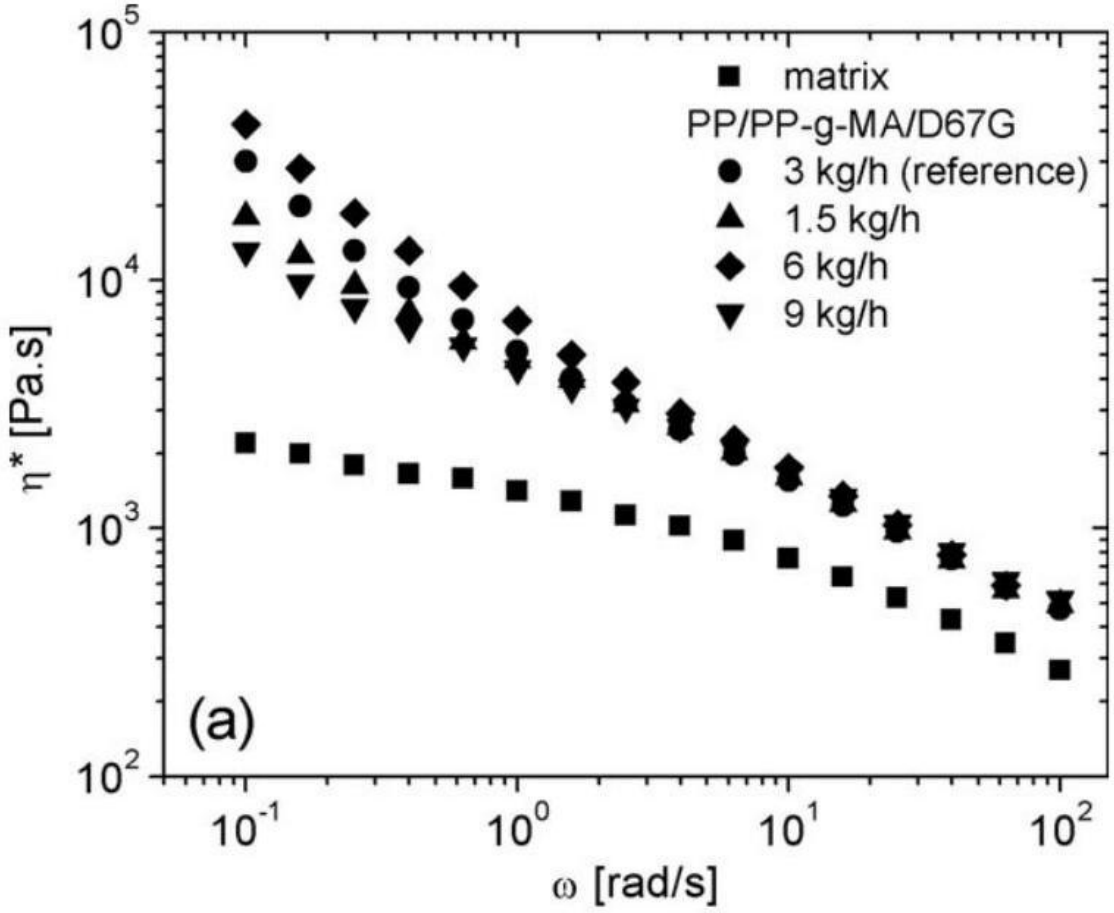
matrix
PP/PP-g-MA/D67G
3 kg/h (reference)
1.5 kg/h
6 kg/h
9 kg/h
(a)
η* [Pa.s]
ω [rad/s]

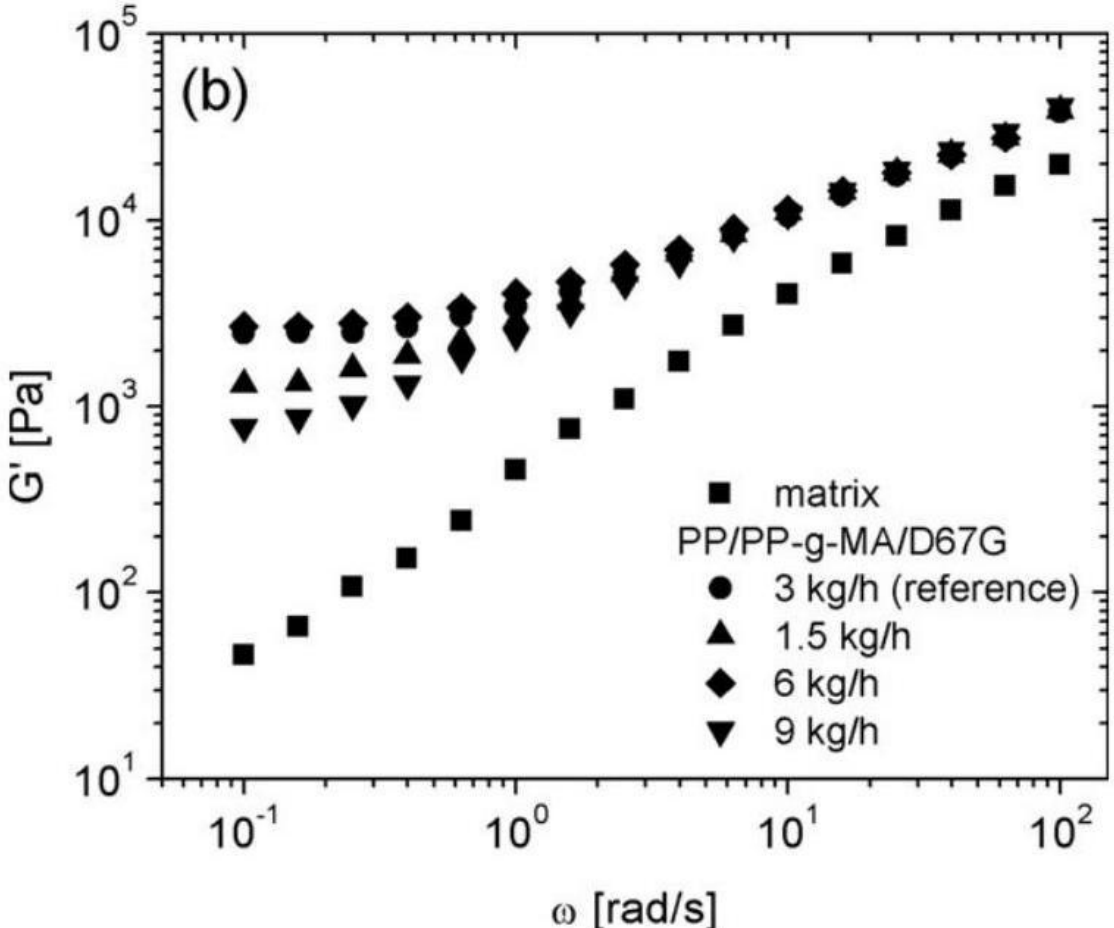
(b)
matrix
PP/PP-g-MA/D67G
3 kg/h (reference)
1.5 kg/h
6 kg/h
9 kg/h
G' [Pa]
ω [rad/s]

Figure 9. Linear viscoelastic response against frequency of the PP/PP- *g* MA/D67G 90/5/5w/w/w nanocomposite prepared with different feed rates. (a) complex viscosity; (b) storage modulus.

8 (as desired), the same applying to bias. These results demonstate the feasibility of using the diffuse reflectance probe for inline real time monitoring of the preparation of polymer-clay nanocomposites directly at the barrel of the extruder, upon its steady-state operation.

Real-Time Monitoring with Diffuse Reflectance

Given the good results reported above, the diffuse reflectance probe was used to monitor in real-time (at the same location as before) the manufacture of the PP/PP- *g*-M A/D67G 90/5/5w/w/ w composite with three distinct feed rates (1.5,6, and 9 kg/h), the other operating conditions remaining constant (barrel and die set to 200°C, screw speed of 100 rpm). As before, 50 spectra were acquired per sample. Although it is well-known that

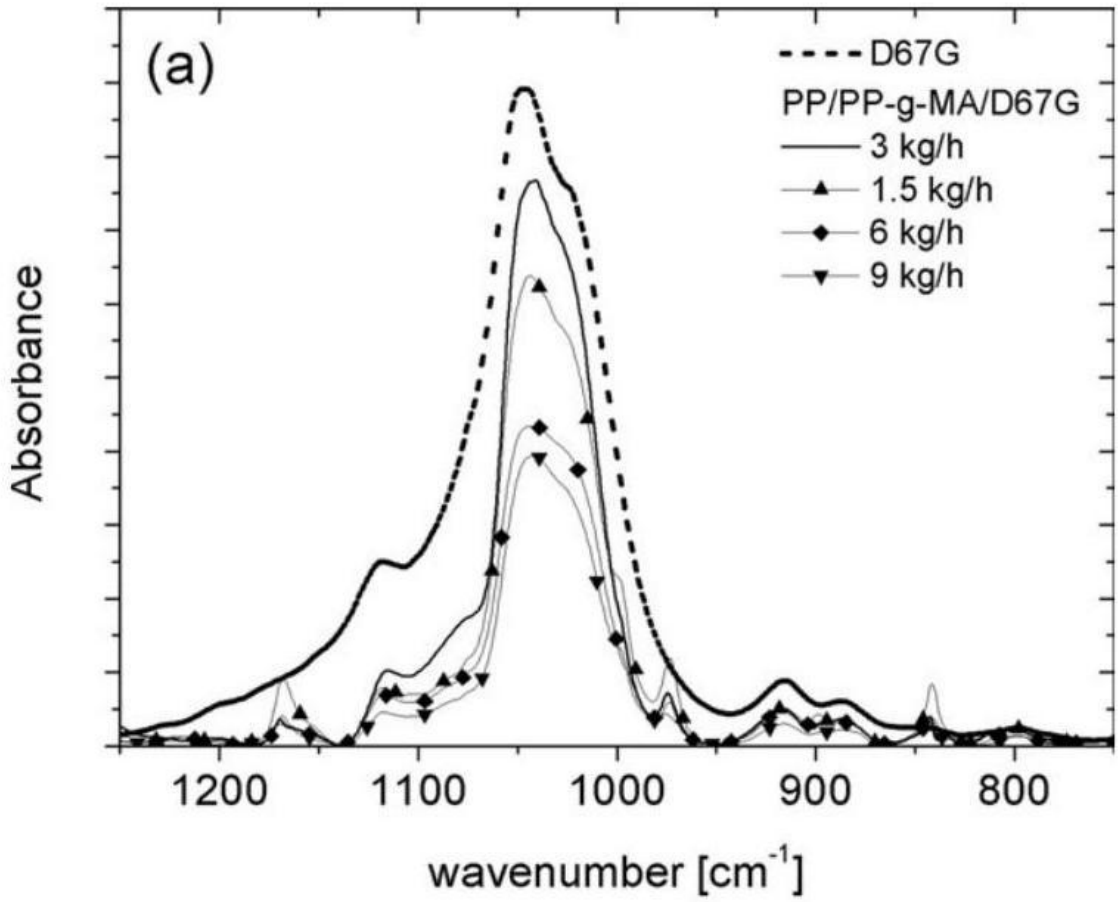
(a)
D67G
PP/PP-g-MA/D67G
3 kg/h
1.5 kg/h
6 kg/h
9 kg/h
Absorbance
1200
1100
1000
900
800
wavenumber [cm-1]

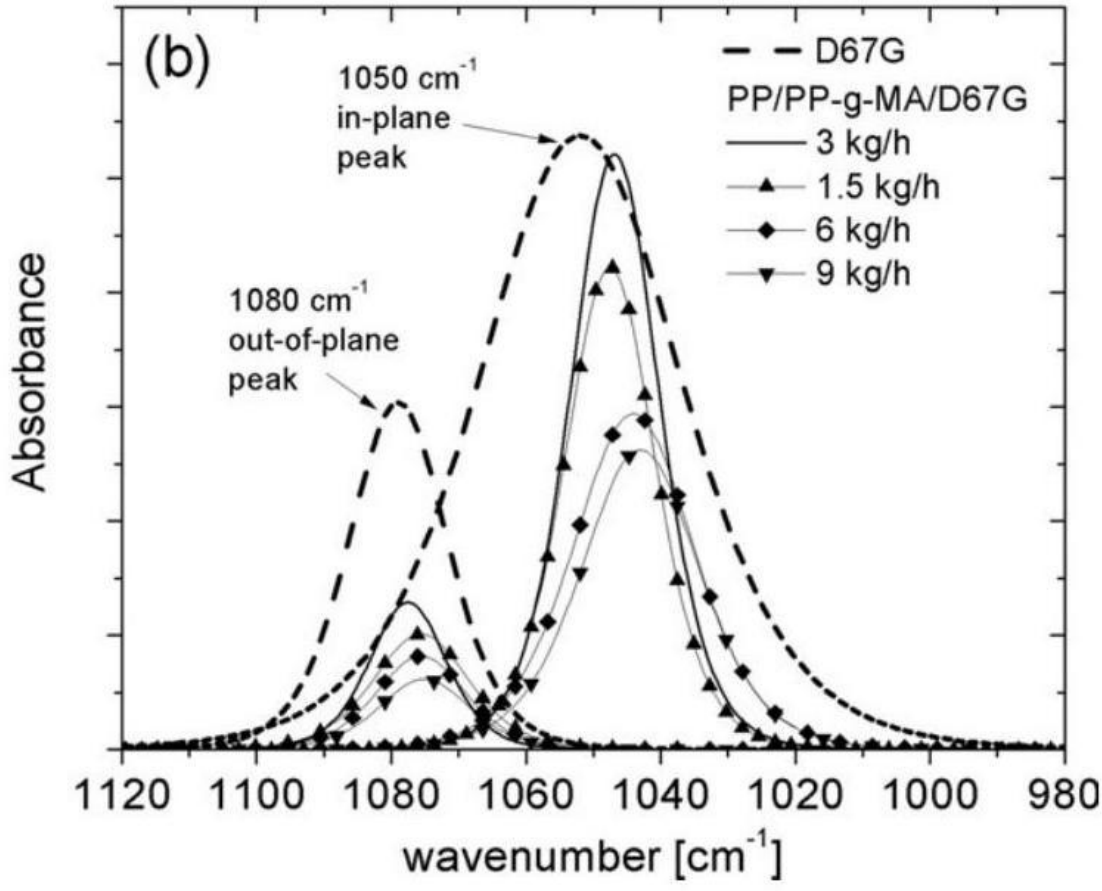
(b)
1050 cm-1
in-plane
peak
1080 cm-1
out-of-plane
peak
D67G
PP/PP-g-MA/D67G
3 kg/h
1.5 kg/h
6 kg/h
9 kg/h
Absorbance
1120
1100
1080
1060
1040
1020
1000
980
wavenumber [cm-1]

Figure 10. FTIR spectra in the Si-O band region of the PP/PP- *g*-MA/ D67G 90/5/5 w/w/w nanocomposite prepared with different feed rates: (a) as measured; (b) 1050 and 1080 cm^{-1} fitted peaks.

Table VII. SME, σ_0, and b for the PP/PP- g -MA/D67G 90/5/5w/w/w Nanocomposite Prepared with Different Feed Rates

Q[kg/h]	1.5	3	6	9
SME[Amp/Q]	2	2.3	2.7	2.7
σ_0[kPa]	1.305	2.736	3.812	0.745
b	-0.625	-0.832	-0.840	-0.487

chemometric models should not be extended to materials or processing conditions laying outside the range used to create them, [30,31] the same model is used here, as one would anticipate that throughput variations will produce an effect on clay dispersion similar to that of screw speed, that is, both are variables influencing the same dispersion mechanism. Table VI ranks the predicted relative degree of dispersion of the samples. Dispersion should not increase strictly with output, a maximum being anticipated at intermediate throughputs. Similarly to the effect of screw speed, this behavior could be due to the conflicting effects of higher hydrodynamic stresses and lower residence times with increasing feed rate. Nevertheless other factors may also come into play, as the higher shear rates associated to the higher outputs boost viscous dissipation and this may trigger polymer degradation. In turn, the degraded material will become less viscous and could outflow from between the clay platelets, thus delaying or even reducing dispersion. At the same location of the in-line measurement, samples were collected from the extruder and characterized off-line. Rheology (complex viscosity, storage modulus) and FTIR data (absorbance) are depicted in Figures 9 and 10, respectively. The SME, σ_0, and b values are shown in Table VII. At low frequencies, the rheological parameters increase with feed rate up to 6 kg/h and decrease for 9 kg/h (Figure 9); identical results are shown for melt yield stress (σ_0) and power law exponent (b). These results are in agreement with those reported by Lertwimolnun and Vergnes [5] for postmortem samples collected along a twin screw extruder. FTIR data (Figure 10) demonstrates that the samples prepared at 6 and 9 kg/h have identical peak shifts. An X-ray diffraction (XRD) analysis of these samples could not detect any significant changes of the clay diffraction pattern with increasing feed rate. However, it is worth to stress again that these techniques used explore different length scales.

In view of the experimental data of Figures 9, 10 and Table VII, the normalized average values for the effect of feed rate are listed in Table VI. The matching between the NIR predictions and the measured values is quite satisfactory, the maximum in dispersion and its value being well predicted.

CONCLUSIONS

The practical feasibility of using diffuse reflectance NIR for the in-line monitoring along the axis of an extruder of the level of clay dispersion during the manufacture of polymer-clay nanocomposites is demonstrated. Consequently, the utilization of several of these

probes positioned along the screw axis and die will characterize the evolution of clay dispersion upon compounding, which would be quite relevant for process set-up, composition tuning, optimization, and control.

Although thus far transmission probes have been preferred for NIR monitoring of polymer melt processes, modern commercial diffuse reflectance probes can be made available with a Dyniscotype threaded tip that enables their simple fixing at any available pressure sensor port of the extruder or die. However, the spectra measurement could be affected by the periodic rotation of the tips of the screw elements, the presence of large clay solid particulates (more likely immediately upon polymer melting) acting as diffuse reflectors, the complex three-dimensional flow pattern in the screw channel and the possibility that the screws will not work locally fully filled. Measurements performed on an empty extruder operating normally demonstrated the maximum absorbance values were less than 0.1% of those measured for the melt, discarding the first effect above. The performance of transmission and diffuse reflectance measurements for the same clay nanocomposite recipes and operating conditions was evaluated. By means of chemometrics, a 7 parameter calibration model was developed for each, using the same off-line characterization data (from oscillatory small amplitude rheology, FTIR and a process-related thermomechanical index). Despite the higher variability of the diffuse reflectance signal due to scattering effects, both models exhibited similar high quality measures.

When the diffuse reflectance probe was used for the real-time monitoring of the effect of feed rate on the dispersion level of the same nanocomposite, the nonlinear effect measured off-line was readily detected.

REFERENCES

1. Ray, S. S.; Okamoto, M. Prog. Polym. Sci. 2003, 28, 1539.
2. Pavlidou, S.; Papaspyrides, C. D. Prog. Polym. Sci. 2008, 33, 1119.
3. Lertwimolnun, W.; Vergnes, B. Polymer 2005, 46, 3462.
4. Lertwimolnun, W.; Vergnes, B. Polym. Eng. Sci. 2006, 46, 314.
5. Lertwimolnun, W.; Vergnes, B. Polym. Eng. Sci. 2007, 47, 2100.
6. Vermogen, A.; Masenelli-Varlot, K.; Séguéla, R.; DuchetRumeau, J.; Boucard, S.; Prele, P. Macromolecules 2005, 38, 9661.
7. Modesti, M.; Lorenzetti, A.; Bon, D.; Besco, S. Polymer 2005, 46, 10237.
8. Mould, S.; Barbas, J. M.; Machado, A. V.; Nóbrega, J. M.; Covas, J. A. Polym. Testing 2011, 30, 602.
9. Durmus, A.; Kasgoz, A.; Macosko, C. W. Polymer 2007, 48, 4492.
10. Alig, I.; Steinhoff, B.; Lellinger, D. Meas. Sci. Technol. 2010, 21, 1.
11. Rodd, T. R. In Handbook of Vibration Spectroscopy; Chalmers, J.M., Griffiths, P.R., Eds; Willey, Chichester, UK, 2002; Vol. 2.
12. Tate, J. D.; Chauvel, P.; Guenard, R. D.; Harner, R. In Handbook of Vibration Spectroscopy; Chalmers, J.M., Griffiths, P.R., Eds; Willey, Chichester, UK, 2002; Vol. 4.

13. Coates, P. D.; Barnes, S. E.; Sibley, M. G.; Brown, E. C.; Edwards, H. G.; Scowen, I. J. Polymer 2003, 44, 5937.
14. George, G.; Hynard, N.; Cash, G.; Rintoul, L.; O'Shea, M. C. R. Chim. 2006, 9, 1433.
15. Hansen, M. G.; Vedula, S. J. Appl. Polym. Sci. 1998, 68, 859.
16. Nagata, T.; Oshima, M.; Tanigaki, M. Polym. Eng. Sci. 2000, 40, 1107.
17. Allig, I.; Fischer, D.; Lellinger, D.; Steinhoff, B. Macromol. Symposia. 2005, 230, 51.
18. Barrès, C.; Bounor-Legaré, V.; Mellis, F.; Michel, A. Polym. Eng. Sci. 2006, 46, 1613.
19. Barnes, S. E.; Sibley, M. G.; Edwards, H. G.; Coates, P. D. Trans. Inst. Meas. Control 2007, 29, 453.
20. Rohe, T.; Kölle, S.; Stern, C.; Eisenreich, N.; Eyerer, P. Recent Res. Devel. Pure Appl. Anal. Chem. 2001, 3, 13.
21. Moghaddam, L.; Martin, D. J.; Halley, P. J.; Fredericks, P. M. Vib. Spectrosc. 2009, 51, 86.
22. Witschnigg, A.; Laske, S.; Kracalik, M.; Feuchter, M.; Pinter, G.; Maier, G.; Märzinger, W.; Haberkorn, M.; Langecker, G. R.; Holzer, C. J. Appl. Polym. Sci. 2010, 117, 3047.
23. Fischer, D.; Müller, J.; Kummer, S.; Kretzschmar, B. Macromol. Symp. 2011, 35, 10.
24. Barbas, J. M.; Machado, A. V.; Covas, J. A. Polym. Testing 2012, 31, 527.
25. Machado, A. V.; Covas, J. A.; Duin, M. J. Appl. Polym. Sci. 1999, 71, 135.
26. Cassagnau, P. Polymer 2008, 49, 2183.
27. Krishnamoorti, R.; Giannelis, E. P. Macromolecules 1997, 30, 4097.
28. Cole, K. C. Macromolecules 2008, 41, 834.
29. Yan, L.; Roth, C. B.; Low, P. F. Langmuir 1996, 12, 4421.
30. Burns, D. A.; Ciurczak, E. W. Eds.; In Handbook of NearInfrared Analysis, CRC Press, Florida, USA, 2008.
31. Xiang, D.; LoBrutto, R.; Cheney, J.; Wabuyele, B. W.; Berry, J.; Lyon, R.; Wu, H.; Khan, M. A.; Hussain, A. S. Appl. Spectrosc. 2009, 63, 33.
32. Saeed, M.; Probst, L.; Betz, G. J. Pharm. Sci. 2011, 100, 1130.
33. Kohlgrüber, K. In Co-rotating twin-screw extruders: Fundamentals, Technology and Applications. Carl Hanser Verlag, Munich, Germany, 2008.
34. Madejová, J.; Pentrák, M.; Pálková, H.; Komadel, P. Vib. Spectrosc. 2009, 49, 211.
35. Dumitrescu, O.; Baker, D. C.; Foster, G. M.; Evans, K. M. Polym. Testing 2005, 24, 367.